Radiation pressure by electron cyclotron waves on density fluctuations

Abhay Ram[1,*] and *Kyriakos* Hizanidis[2,**]

[1]Plasma Science and Fusion Center, Massachusetts Institute of Technology, Cambridge, MA 02139. USA
[2]National Technical University of Athens, 157 73 Zographou, Greece

Abstract. The presence of turbulence in the form of large density fluctuations and coherent filamentary structures in the edge region of fusion plasmas has been well documented. Radio frequency waves, launched from structures near the wall of a tokamak, have to propagate through this turbulent plasma before reaching the core. These density fluctuations can reflect, refract, and diffract the electromagnetic waves, thereby modifying the flow of energy and momentum to the core plasma. Conversely, the radiation pressure of the radio frequency waves can modify the turbulence, whether it is in the edge region or in the core. This article examines some consequences of the radiation force induced by electron cyclotron waves in plasmas. The effect of waves on two different representations of density fluctuations are studied. In the first representation, suitable for both edge and core plasmas, it is assumed that a planar interface separates two different density regimes. The physics basis for the radiation force on an interface separating two different scalar dielectric media was first elucidated by Poynting in 1905 [J. H. Poynting, The London, Edinburgh, and Dublin Philosophical Magazine and Journal of Science **9**, 393-406 (1905)]. Poynting's results are explained within the context of Snell's law and Fresnel equations, and, subsequently, extended to magnetized plasmas. The analysis shows that electron cyclotron waves lead to peaking of the density profile – the interface is pushed towards the region of higher density. The planar interface approximation is the basis of Kirchhoff theory [P. Beckmann and A. Spizzichino, *The Scattering of Electromagnetic Waves from Rough Surfaces* (Artech, Massachusetts, 1987) Chapter 3] used to study wave scattering by turbulent media. In the second representation, appropriate for coherent structures in edge plasmas, the radiation force on a cylindrical filament embedded in a background plasma is determined using the Maxwell stress tensor. A detailed study reveals that the radiation force has a different effect on filaments – those with densities higher than the background density are pulled in towards the source launching the waves, while the lower density filaments are pushed away. The reaction on a filament is large enough to be observed experimentally.

1 Introduction

The edge plasma of toroidal fusion devices is replete with large density fluctuations in the form of turbulence and filamentary structures. The effect of such fluctuations on the propagation of radio frequency (RF) waves has been extensively studied theoretically and computationally [1–7]. Fluctuations tend to scatter RF waves through reflections, refractions, and diffractions. On the other hand, the radiation pressure of electromagnetic RF waves can have an impact on density fluctuations [8]. In this paper we discuss some of our initial thoughts and ideas on RF induced radiation pressure; specifically, by waves in the electron cyclotron (EC) range of frequencies. In section 2 we set up the physics basis of radiation pressure at an interface separating two scalar dielectric media. The transition to interfaces separating two different electron densities in a magnetized plasma is carried out in section 3. The permittivity of a plasma is a tensor but the physical consequences of the radiation force are similar to those in a scalar dielectric. Planar interfaces are not a good representation of turbulent structures that manifest themselves as filament or blobs – the geometry of the scatterer plays a role in the scattering process. In section 4, we model the scattering of EC waves by a cylindrical filament. The radiation force is evaluated using the Maxwell stress tensor and found to exhibit properties which are in contrast to those for planar interfaces. Besides reflection and transmission, common to planar interfaces, a filament leads to side-scattering, diffraction, and shadowing, as well as non-planar wave fields within the filament. Consequently, there is angular variation of the stress force along the interface which, in turn, changes the physics of the forces acting on the surface of a filament. Even though the theoretical analysis is for a step-function transition between two different plasma densities, numerical simulations have shown that there is no significant difference if the transition is smooth [4].

2 Radiation pressure at an interface separating two dielectrics

Consider a planar interface in the y-z plane at $x = 0$ that separates two different scalar dielectric media with refrac-

*e-mail: abhay@mit.edu
**e-mail: kyriakos@central.ntua.gr

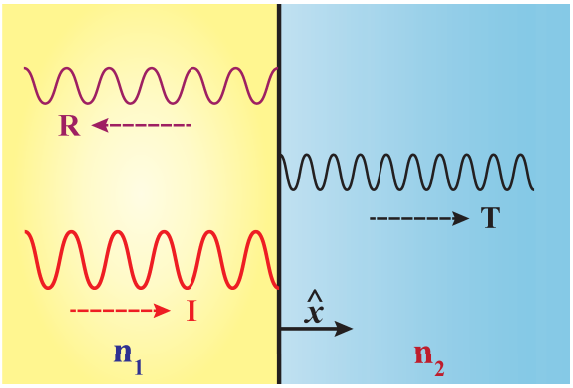

Figure 1. The scattering of an incident I wave to a reflected R and transmitted (refracted) T wave at an interface separating two different scalar dielectrics with refractive indices n_1 and n_2. The interface is in the y-z plane; $\hat{x}$ is the outward pointing normal to the surface.

tive indices n_1 and n_2 (figure 1). The normal to the interface is along $\hat{x}$ while $\hat{z}$ is normal to the plane of the figure. A plane electromagnetic wave (I) incident on the interface will get scattered into a reflected (R) and transmitted (T) plane waves. The electric field of an incident wave propagating along $\hat{x}$ is $\vec{E}_I = E_{I0}\, e^{ik_1 x - i\omega t}\, \hat{y}$, where E_{I0} is the amplitude of the wave, k_1 is the magnitude of the propagation vector along $\hat{x}$, ω is the angular frequency of the wave, and $(\hat{x}, \hat{y}, \hat{z})$ are the unit vectors along the (x, y, z) directions, respectively. From Snell's law, the reflected and the transmitted waves will also propagate along $\hat{x}$, and their electric fields are $\vec{E}_R = E_{R0}\, e^{-ik_1 x - i\omega t}\, \hat{y}$ and $\vec{E}_T = E_{T0}\, e^{ik_2 x - i\omega t}\, \hat{y}$, respectively. Here E_{R0} and E_{T0} are the electric field amplitudes of the reflected and transmitted waves, respectively, and k_2 is the magnitude of the propagation vector of the transmitted wave along $\hat{x}$. From Maxwell's equations, $\omega = v_1 k_1$ and $\omega = k_2 v_2$ are the dispersion relations for the waves in the two dielectric media; $v_1 = c/n_1$ and $v_2 = c/n_2$ with c being the speed of light in vacuum. The continuity of the tangential components of the electric and magnetic fields at the interface yields the Fresnel equations [9],

$$\frac{E_R}{E_I} = \frac{n_1 - n_2}{n_1 + n_2}, \qquad \frac{E_T}{E_I} = \frac{2n_1}{n_1 + n_2}. \tag{1}$$

The energy, or Poynting, flux averaged over one time period $2\pi/\omega$ is,

$$\left\langle \vec{S} \right\rangle = \frac{1}{2\mu_0} \mathrm{Re}\left(\vec{E} \times \vec{B}^*\right), \tag{2}$$

where μ_0 is the vacuum permeability. For waves in scalar dielectrics $\left\langle \vec{S} \right\rangle \parallel \vec{k} \parallel \hat{x}$. The reflection and transmission coefficients are, respectively,

$$R = \frac{|\langle S_x \rangle_R|}{|\langle S_x \rangle_I|} = \left(\frac{n_1 - n_2}{n_1 + n_2}\right)^2, \tag{3}$$

$$T = \frac{|\langle S_x \rangle_T|}{|\langle S_x \rangle_I|} = \frac{n_2}{n_1}\left(\frac{2n_1}{n_1 + n_2}\right)^2, \tag{4}$$

where the subscript x indicates that the Poynting vector is along $\hat{x}$. From equations (3) and (4) it is straightforward to show that $R + T = 1$ – a statement on energy conservation.

The time-averaged momentum flux is defined as,

$$\left\langle \vec{\mathcal{P}} \right\rangle = \frac{\left\langle \vec{S} \right\rangle}{v}, \tag{5}$$

where v is the speed of light in a dielectric medium. The normalized momenta for the reflected and transmitted waves are, respectively,

$$P_R = \frac{\langle \mathcal{P}_x \rangle_R}{\langle \mathcal{P}_x \rangle_I} = -\left(\frac{n_1 - n_2}{n_1 + n_2}\right)^2, \tag{6}$$

$$P_T = \frac{\langle \mathcal{P}_x \rangle_T}{\langle \mathcal{P}_x \rangle_I} = \frac{n_2^2}{n_1^2}\left(\frac{2n_1}{n_1 + n_2}\right)^2. \tag{7}$$

The negative sign in equation (6) is an indication that the reflected wave is propagating in a direction opposite to the incident wave. From equations (6) and (7), we note that $P_R + P_T \neq 1$; i.e., momentum is not conserved. Since neither dielectric allows for momentum dissipation, it is evident that the difference is the momentum P_B imparted to the interface. From momentum conservation,

$$P_B = \frac{\langle \mathcal{P}_x \rangle_B}{\langle \mathcal{P}_x \rangle_I} = 1 - P_R - P_T = 2\left(\frac{n_1^2 - n_2^2}{n_1^2 + n_2^2}\right). \tag{8}$$

P_B is a measure of the radiation force on the interface. From equation (8) we note that if $n_2 > n_1$, the force is in the $-\hat{x}$ direction, while if $n_1 > n_2$ it is in the $+\hat{x}$ direction. In other words, the force on the interface is always directed away from the medium with the higher refractive index. This interesting result was first noted by John Henry Poynting in 1905 [10]. In the paper Poynting states the following: "In any real refraction with ordinary light, there will be reflexion as well as refraction. The reflexion always produces a normal pressure, and the refraction a normal pull. But with unpolarized light, a calculation shows that the refraction pull, for glass at any rate, is always greater than the reflexion push, even at grazing incidence." The "push" and "pull" are with respect to the incoming wave which, with respect to figure 1, correspond to $+\hat{x}$ and $-\hat{x}$, respectively. For vacuum waves incident on a glass surface $n_2 > n_1$, and (8) confirms Poynting's observation. We would like to note that Poynting's argument was based on Planck's relation between energy and frequency, and not on the analysis given above. His reasoning can be interpreted as follows. The transmitted and reflected waves originate from the interface. From Newton's third law, the acquired momentum for each wave exerts a recoil force on the interface. The shorter wavelength wave has larger momentum associated with it; hence, the recoil force due to this wave dominates. For electromagnetic waves incident on a glass interface from vacuum, the transmitted wave has a shorter wavelength. Hence, the interface moves towards the vacuum region. The same argument holds for waves incident on the interface from inside the glass.

3 Radiation pressure at an interface separating two different electron densities in a magnetized plasma

In this section we extend the analysis on radiation pressure for simple dielectrics to a cold, magnetized plasmas. Referring to figure 1, the regions n_1 and n_2 correspond to two different electron densities. We assume that the magnetic field is uniform and pointing along $\hat{z}$, $\vec{B}_0 = B_0\hat{z}$.

3.1 Cold plasma dispersion relation

The dispersion tensor for plane electromagnetic waves propagating in a cold, magnetized plasma is [11],

$$\overleftrightarrow{\mathbf{D}} = \frac{c^2}{\omega^2}\left(\vec{k}\vec{k} - k^2\overleftrightarrow{\mathbf{I}}\right) + \overleftrightarrow{\mathbf{K}}, \tag{9}$$

where $\overleftrightarrow{\mathbf{I}}$ is the identity tensor, and $\vec{k}\vec{k}$ is a dyadic. The permittivity tensor $\overleftrightarrow{\mathbf{K}}$ is,

$$\overleftrightarrow{\mathbf{K}} = \begin{pmatrix} K_{xx} & -iK_{xy} & 0 \\ iK_{xy} & K_{xx} & 0 \\ 0 & 0 & K_{zz} \end{pmatrix}, \tag{10}$$

where,

$$\begin{aligned} K_{xx} &= 1 - \frac{\omega_{pe}^2}{\omega^2 - \omega_{ce}^2} - \sum_i \frac{\omega_{pi}^2}{\omega^2 - \omega_{ci}^2}, \\ K_{xy} &= -\frac{\omega_{ce}}{\omega}\frac{\omega_{pe}^2}{\omega^2 - \omega_{ce}^2} + \sum_i \frac{\omega_{ci}}{\omega}\frac{\omega_{pi}^2}{\omega^2 - \omega_{ci}^2}, \\ K_{zz} &= 1 - \frac{\omega_{pe}^2}{\omega^2} - \sum_i \frac{\omega_{pi}^2}{\omega^2}, \end{aligned} \tag{11}$$

ω_{pe} (ω_{pi}) and ω_{ce} (ω_{ci}) are the electron (ion) angular plasma and angular cyclotron frequencies, respectively, and the summation is over all the ion species in the plasma. The dispersion relation for waves in the plasma is given by $\mathcal{D}\left(\vec{k},\omega\right) \equiv \det\left(\overleftrightarrow{\mathbf{D}}\right) = 0$, where det denotes the determinant of the second rank tensor. Without loss of generality, we choose $\vec{k} = k_\perp\,\hat{x} + k_\parallel\,\hat{z}$ – for a homogeneous medium, a simple rotation about the z-axis will ensure this particular form. Assuming that $k_\parallel$, ω, ω_{pe}, ω_{pi}, ω_{ce}, and ω_{ci} are all prescribed, the dispersion relation $\mathcal{D}(k_\perp, k_\parallel, \omega) = 0$ is biquadratic in $k_\perp$. A representative solution of the dispersion relation for EC waves in a cold plasma is plotted in figure 2. There are two primary differences between scalar and anisotropic tensor permittivities. First, the former has a dispersion relation that is quadratic in k while the latter is biquadratic in $k_\perp$. Thus, there is an additional wave that is a normal mode in a plasma. Second, for waves in scalar dielectrics, $\vec{k}$, $\vec{E}$, and $\vec{B}$ are normal to each other. The continuity of tangential $\vec{E}$ and $\vec{B}$ at the interface leads to two independent boundary conditions. For plasma waves, it is $\vec{k}$, $\vec{D} = \epsilon_0\overleftrightarrow{\mathbf{K}}.\vec{E}$, and $\vec{B}$ that are normal to each other; $\vec{D}$ is the electric displacement field and ϵ_0 is the vacuum permittivity. Combined with the anisotropy of the permittivity tensor, the continuity of tangential $\vec{E}$ and $\vec{B}$ at an interface

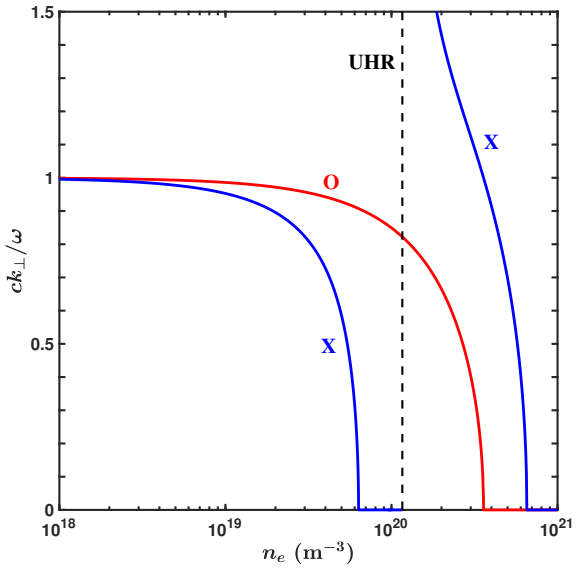

Figure 2. Dispersion properties of EC waves obtained from $\mathcal{D}(k_\perp, k_\parallel, \omega) = 0$: $ck_\perp/\omega$ is plotted as a function of the electron density for $f = \omega/2\pi = 170$ GHz, $B_0 = 5$ T, and $k_\parallel = 0$. The labels indicate the extraordinary X mode, the ordinary O mode, and the upper hybrid resonance UHR. The X mode is cutoff at $n_e \approx 6.34 \times 10^{19}$ m^{-3}, the UHR is located at $n_e \approx 1.15 \times 10^{20}$ m^{-3}, the O mode is cutoff at $n_e \approx 3.58 \times 10^{20}$ m^{-3}, and the second X mode is cutoff at $n_e \approx 6.53 \times 10^{20}$ m^{-3}.

leads to four independent boundary conditions [2]. This is consistent with the presence of two distinct waves in a plasma. As depicted in figure 3, the scattering of an incident wave by an interface separating two different densities in a magnetized plasma leads to two reflected and two transmitted waves. For electron cyclotron waves, regardless of the incident wave, the scattered waves are the extraordinary X and the ordinary O waves.

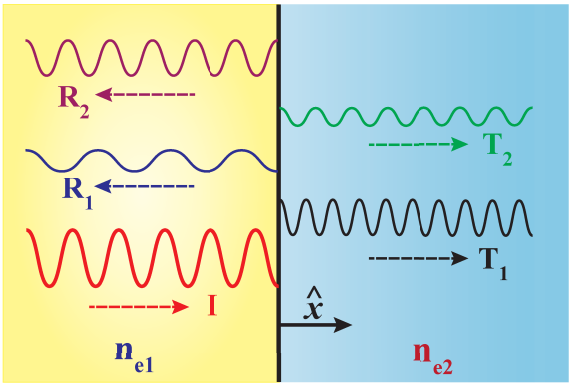

Figure 3. In contrast to figure 1, the scattering of an incident I wave at an interface separating two different electron densities, n_{e1} and n_{e2}, in a uniformly magnetized plasma results in two reflected, R_1 and R_2, and two transmitted, T_1 and T_2, waves.

3.2 Scattering and radiation pressure

We follow the same procedure as in section 2 to determine the radiation pressure at an interface separating two dif-

ferent electron densities. For the parameters indicated in figure 2, the direction of propagation of the incident wave – whether it is the O mode or the X mode – is normal to the interface. For this particular case, the scattered waves are the same as the incident wave; e.g., for an incident X mode the scattered waves are also X modes. The time-averaged Poynting flux is given by (5) in which v is replaced by the phase speed of the wave $\omega/k_\perp$ [12]. We assume that the incident wave, either the O mode or the X mode, is approaching the interface from a region with density n_{e1}. Below we present results for three different combinations of n_{e1} and n_{e2} (figure 3).

3.2.1 $n_{e1} < n_{e2}$ with O and X modes propagating in both regions

For $n_{e1} = 8\times10^{18}$ m^{-3} and $n_{e2} = 10^{19}$ m^{-3}, figure 2 shows that the O and X modes are propagating on either side of the interface. The momentum transfer to the interface is obtained by matching the wave phases and the transverse componets of the wave electric and magnetic fields at the interface. We find that the normalized momentum transfer is,

$$P_{BO} \;=\; 2.86\times10^{-3}, \qquad P_{BX} \;=\; 1.06\times10^{-2}, \quad (12)$$

for an incident O mode and an incident X mode, respectively. The absolute values do not have an experimental significance at this point; we will put these numbers into proper context when we consider the radiation pressure on a well-defined cylindrical filament. However, two observations stand out. First, from the positive sign in front of the numerical values, we realize that both the X and O modes push the higher density region away from the antenna that launches these waves. This is in complete agreement with the direction of the momentum imparted to an interface separating two different scalar dielectrics when the electromagnetic wave is incident from a region of higher refractive index. For simple dielectrics, the index of refraction increases with density; see, for example, [13]. For plasmas, as shown in figure 2, the index of refraction decreases with density. Second, the push due to the incident X mode is stronger than that for the O mode.

3.2.2 $n_{e1} > n_{e2}$ with O and X modes propagating in both regions

Here we consider the case when the initial wave is incident at the interface from a region of lower density. Let $n_{e1} = 10^{19}$ m^{-3} and $n_{e2} = 8\times10^{18}$ m^{-3}– this is a reversal of the parameters in section 3.2.1. The normalized momentum transfer to the interface is,

$$P_{BO} \;=\; -2.86\times10^{-3}, \qquad P_{BX} \;=\; -1.06\times10^{-2}, \quad (13)$$

for an incident O mode and an incident X mode, respectively. The negative sign indicates that the interface is pulled towards the antenna. Again, this is consistent with the intuition developed from scalar dielectrics. As in section 3.2.1, the magnitude of the momentum due to the X mode is larger than that due to the O mode.

3.2.3 $n_{e1} < n_{e2}$ – total internal reflection of the X mode

From figure 2, we note that the X mode is cutoff at a density below the upper hybrid resonance. We examine the affect of this cutoff on wave scattering by choosing $n_{e1} = 5\times10^{19}$ m^{-3} and $n_{e2} = 7\times10^{19}$ m^{-3}; in the first region both modes are propagating while in the second region the X mode is cutoff. For an incident O mode or X mode, the normalized momentum transfer to the interface is, respectively,

$$P_{BO} \;=\; 0.314, \qquad P_{BX} \;=\; 2.. \quad (14)$$

The direction of the momentum for the O mode is in line with our previous reasoning. For the X mode, the incident wave is completely reflected and, because of normal incidence, there is no transfer of momentum to the O mode. The physics for total reflection of the X mode is similar to an elastic collision of a ball with a wall – the momentum imparted to the wall is twice the incoming momentum of the ball.

4 Radiation pressure on a cylindrical filament

The scattering of waves by an infinite plane simplifies the associated algebra while providing an insight into the physics of radiation pressure on the plane. When the scatterer is not an infinite plane, geometrical effects become important because boundary conditions on the electromagnetic fields have to be satisfied on the surface of scatterer. The edge region of fusion plasmas is populated with blobs and filaments [14] which can alter the propagation of RF waves and, in turn, be influenced by the radiation pressure of these waves.

4.1 Basic description of wave scattering by a cylindrical filament

We assume a cylindrical plasma filament of radius a, embedded in a uniform background, with its axis aligned along the magnetic field line. The density inside the filament is constant and different from the background density. The whole system is in a homogeneous magnetic field. The wave propagation is given by the Faraday-Ampere equation,

$$\nabla\times\left(\nabla\times\vec{E}\,(\vec{r})\right) - \frac{\omega^2}{c^2}\,\overleftrightarrow{\mathbf{K}}\,(\vec{r})\;.\,\vec{E}\,(\vec{r}) \;=\; 0, \quad (15)$$

where the time dependence of all fields is of the form $\exp(-i\omega t)$. The propagation vector of the incident RF wave is in the x-y plane and of the form $\vec{k} = k_\perp\hat{x} + k_\parallel\hat{z}$ with $\hat{x}$ and $\hat{z}$ being the unit vectors along the x and z directions, respectively. The Faraday-Ampere equation is solved in cylindrical coordinates subject to the boundary conditions [2],

$$\hat{\rho}\times\left(\vec{E}_I + \vec{E}_S\right)\Big|_{\rho=a} \;=\; \hat{\rho}\times\vec{E}_F\Big|_{\rho=a}, \quad (16)$$

$$\hat{\rho}\times\left(\vec{B}_I + \vec{B}_S\right)\Big|_{\rho=a} \;=\; \hat{\rho}\times\vec{B}_F\Big|_{\rho=a}, \quad (17)$$

where $\hat{\rho}$ is the outward pointing normal vector at the interface of the filament, ρ is the radial coordinate, and all fields are evaluated at the surface of the filament $\rho = a$. The subscripts I, S, and F denote the incoming RF field, the scattered field (outside the filament), and the field inside the filament, respectively. A sample result for the scattering is shown in figure 4 where an incident O mode is scattered by a filament of radius 1 cm. The parameters are as outlined in the caption. The filament leads to some reflection, refraction, diffraction, side-scattering, and shadowing. Even though the incoming wave is a plane wave, it is evident that the scattered fields are not plane waves. This is exemplified in figure 5 showing details of the field structure inside the filament.

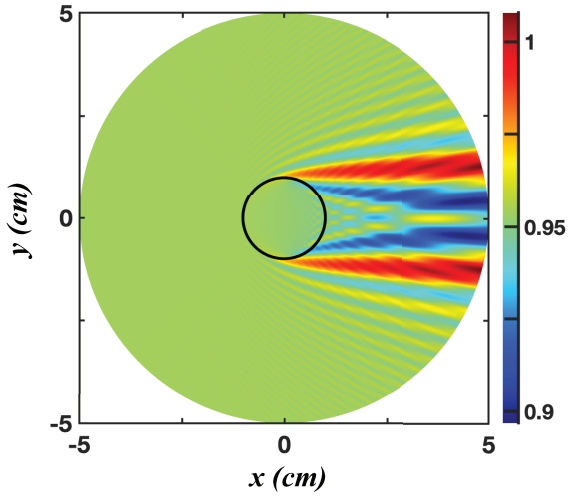

Figure 4. Scattering of an O mode, incident from the left, by a filament of radius 1 cm centered at the origin. The normalized, time-averaged Poynting flux in the x-direction $< S_x > / | < \vec{S}_I > |$ is plotted in the x-y plane; $\vec{S}_I$ is the total Poynting vector of the incident wave. The electron density of the background plasma is $n_{eb} = 5 \times 10^{18}$ m^{-3} while inside the filament it is $n_{ef} = 6.5 \times 10^{18}$ m^{-3}; the wave frequency is 170 GHz, the magnetic field is 5 T and pointing in the z direction, and the incoming wave has $ck_{\|}/\omega = 0.3$.

4.2 Radiation force – Maxwell stress tensor

The electromagnetic fields obtained from the scattering equations (15)-(17) can be used to evaluate the Maxwell stress tensor and, subsequently, the radiation force on the filament [12, 15]. For the complex fields, the stress tensor is,

$$\overleftrightarrow{\mathbf{T}} = \vec{E}_R\vec{D}_R + \vec{H}_R\vec{B}_R - \frac{1}{2}\left(\vec{E}_R \cdot \vec{D}_R + \vec{H}_R \cdot \vec{B}_R\right)\overleftrightarrow{\mathbf{I}}, \quad (18)$$

where the subscript R indicates the real part of the associated field; the first two terms on the right hand side are dyadics, $\overleftrightarrow{\mathbf{I}}$ is the identity tensor, $\vec{H}$ is the magnetic intensity, and $\vec{B} = \mu_0\vec{H}$. Using the relationship between $\vec{D}$ and $\vec{E}$, the time average over one period of the wave cycle yields,

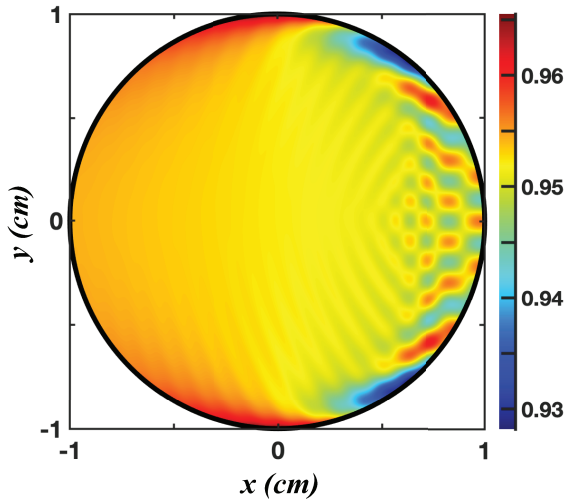

Figure 5. A magnified view of the normalized, time-averaged Poynting flux inside the filament.

$$\left\langle \overleftrightarrow{\mathbf{T}} \right\rangle = \frac{1}{2}\,\mathrm{Re}\left[\epsilon_0 \vec{E}\,\overleftrightarrow{\mathbf{K}}^* \cdot \vec{E}^* + \mu_0 \vec{H}\vec{H}^* - \frac{1}{2}\left(\epsilon_0 \vec{E} \cdot \overleftrightarrow{\mathbf{K}}^* \cdot \vec{E}^* + \mu_0 \left|\vec{H}\right|^2\right)\overleftrightarrow{\mathbf{I}}\right], \quad (19)$$

where Re indicates the real part and * the complex conjugate.

In the cylindrical coordinate system, the time-averaged force on a filament of axial length L is [12, 16],

$$\overrightarrow{\mathcal{F}} = \int \left\langle \overleftrightarrow{\mathbf{T}} \right\rangle \cdot d\boldsymbol{A} = a \int_0^L \int_0^{2\pi} \left\langle \overleftrightarrow{\mathbf{T}}(\rho = a) \right\rangle \cdot \hat{\rho}, \quad (20)$$

where the elemental area on the surface of the filament is $d\boldsymbol{A} = a\, d\phi\, dz\, \hat{\rho}$, with ϕ being the azimuthal coordinate around the axis of the filament. On the surface of the filament,

$$\left\langle \overleftrightarrow{\mathbf{T}}(\rho = a) \right\rangle \cdot \hat{\rho} = \left\langle \overleftrightarrow{\mathbf{T}}(\rho = a) \right\rangle_b \cdot \hat{\rho} - \left\langle \overleftrightarrow{\mathbf{T}}(\rho = a) \right\rangle_f \cdot \hat{\rho}, \quad (21)$$

where the subscript b indicates that the tensor is evaluated for the fields in the background plasma – the incident and the scattered fields, and the subscript f is for fields inside the filament. The negative sign on the right hand side is due to the inward pointing normal for the filamentary fields. Equation (21) is a vector equation whose cylindrical components are determined using the boundary conditions (16) and (17). After some algebra we find that,

$$\hat{\rho} \cdot \left\langle \overleftrightarrow{\mathbf{T}}(\rho = a) \right\rangle \cdot \hat{\rho} = \frac{\epsilon}{4}\left[K_{xx}^B \left|E_{I\rho} + E_{S\rho}\right|^2 - K_{xx}^F \left|E_{F\rho}\right|^2 + \left(K_{xx}^F - K_{xx}^B\right)\left|E_{F\phi}\right|^2 + \left(K_{zz}^F - K_{zz}^B\right)|E_{Fz}|^2\right]_{\rho=a}, \quad (22)$$

$$\hat{\phi} \cdot \left\langle \overleftrightarrow{\mathbf{T}}(\rho = a) \right\rangle \cdot \hat{\rho} = 0, \quad (23)$$

$$\hat{z} \cdot \left\langle \overleftrightarrow{\mathbf{T}}(\rho = a) \right\rangle \cdot \hat{\rho} = 0. \quad (24)$$

The superscripts B and F indicate that these elements of the permittivity tensor are evaluated for plasma parameters corresponding to the background and filamentary plasmas, respectively. The subscripts in the electric fields include the components corresponding to the cylindrical coordinate system. The right hand side is evaluated at the surface of the filament. From equations (23)-(24) we note that the RF fields do not induce any shear forces on the filament; the only force is in the radial direction. The radial component (22) is a function of the azimuthal angle ϕ and is independent of z; the z variation of the fields is $\exp(ik_z z)$ and is accounted for in the matching of wave phases at the surface of the filament. The radial force can lead to two possible effects – spatial displacement of the filament and its azimuthal distortion.

The only component of $\vec{F}$ in (20) is in the $\hat{\rho}$ direction. Since (22) has no variation along z, the radial force per unit axial length has two Cartesian components in the x and y directions,

$$\begin{pmatrix}\mathcal{F}_x\\ \mathcal{F}_y\end{pmatrix} = a\int_0^{2\pi} d\phi \begin{pmatrix}\cos\phi\\ \sin\phi\end{pmatrix} \hat{\rho}\cdot\left\langle \overleftrightarrow{\mathbf{T}}(\rho=a)\right\rangle\cdot\hat{\rho}. \qquad (25)$$

We have redefined the force vector in (20) as force per unit axial length.

The power flux of the incident wave is

$$S_I = \left|\left\langle \vec{S}_I\right\rangle\right| = \frac{1}{2}\sqrt{\frac{\epsilon_0}{\mu_0}}\,|\mathcal{E}_0|^2 \qquad (26)$$

where $\left\langle \vec{S}_I\right\rangle$ is the time-averaged Poynting vector and $\mathcal{E}_0$ is the electric field amplitude – both for the incident wave. The force on a filament per unit incident power flux is,

$$\begin{pmatrix}\widetilde{\mathcal{F}}_x\\ \widetilde{\mathcal{F}}_y\end{pmatrix} = \frac{1}{S_I}\begin{pmatrix}\mathcal{F}_x\\ \mathcal{F}_y\end{pmatrix}\ \frac{\mathrm{N\ m^{-1}}}{\mathrm{W\ m^{-2}}}. \qquad (27)$$

The units expressed on the right hand side are Newton per meter (of axial length) for the force and Watt per square meter for the power flux. The stress force on the filament induces an acceleration,

$$\begin{pmatrix}\mathfrak{a}_x\\ \mathfrak{a}_y\end{pmatrix} = \frac{1}{\mathfrak{m}}\begin{pmatrix}\widetilde{\mathcal{F}}_x\\ \widetilde{\mathcal{F}}_y\end{pmatrix}, \qquad (28)$$

where $\mathfrak{m}$ is the mass of a cylindrical filament of length 1 m and radius a m.

4.3 Radiation force – numerical results

The analytical results in section 4.2 are used to illustrate various properties of the radiation force induced by EC waves on a filament of plasma. The primary term in calculating the force is the integrand in (25), $\left\langle T_{\rho\rho}\right\rangle \equiv \hat{\rho}\cdot\left\langle \overleftrightarrow{\mathbf{T}}\right\rangle\cdot\hat{\rho}$, given explicitly in (22). Figure 6 shows the variation of $c\left\langle T_{\rho\rho}\right\rangle/S_I$ as a function of ϕ along the surface of the filament. The variation along ϕ shows the radiation force is not uniform; the negative sign is an indication that the force is pulling the filament towards the source that launched the O mode.

In obtaining the results that follow, we assume a plasma containing deuterons as the single ion species. Then the mass of a filament 1 m long is $\mathfrak{m} = 1.05\times 10^{-26}\, a^2\, n_{ef}$ kg, where n_{ef} is the electron density inside the filament. Furthermore, we set $a = 0.01$ m, $B_0 = 5$ T, and wave frequency at 170 GHz. There is an important point that needs to be made here – from all numerical simulations that we have carried out for different density regimes and, notably, for different waves (ion cyclotron, helicon, and lower hybrid waves), we find $\mathfrak{a}_y = 0$ [8]. Consequently, we will display results for $\mathfrak{a}_x$ only.

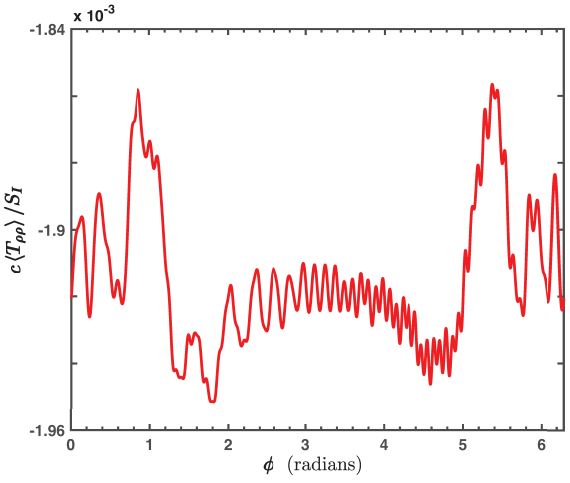

Figure 6. Radial force on the filament surface normalized to the power flux of the incident wave versus the azimuthal angle. The incident wave is an O mode and the parameters are the same as for figure 4.

4.3.1 *Density inside the filament greater than the background density*

For an EC wave incident from a low density region and interacting with a higher density filament, we set the electron density in the background plasma and inside the filament to be $n_{eb} = 5\times 10^{18}$ m^{-3} and $n_{ef} = 6.5\times 10^{18}$ m^{-3}, respectively. The stress force induced acceleration of the filament is plotted as a function of the parallel index of refraction $ck_\parallel/\omega$ for the O (blue) and X (red) modes in figure 7. The evaluated acceleration is for an incident power $S_I = 1$ kW m^{-2}. There are several points of note. The acceleration induced by the X mode is larger than that by the O mode. In both cases, the acceleration is negative which implies that the filament, which has a higher density relative to the background density, is being pulled in towards the source. This is a significant departure from the results obtained for planar scattering, where a wave incident from the low density region pushed the interface towards the higher density region. The difference can be attributed to the finite geometry of the scatterer – the bounded waves inside the filament are akin to cavity modes built from waves propagating in all directions. At the boundary, the internal modes couple to non-planar scattered fields. Consequently, the entire field structure does not possess the

Cartesian symmetry of the plane incoming wave. The azimuthal variation of the fields lacks uniformity and modifies the direction of the radiation force – figure 6 was an early sign of this feature.

For $ck_{\|}/\omega = 0.9$, the X mode is a propagating mode inside the filament, while for $ck_{\|}/\omega = 0.95$ it becomes evanescent. This change in the propagation of X mode results in a reversal of the slope. In contrast, for a planar interface, section 3.2.3, the X mode underwent total internal reflection. For $ck_{\|}/\omega \lessapprox 0.9$ the magnitude of the force decreases with $k_{\|}$ for the O mode, while it increases for the X mode.

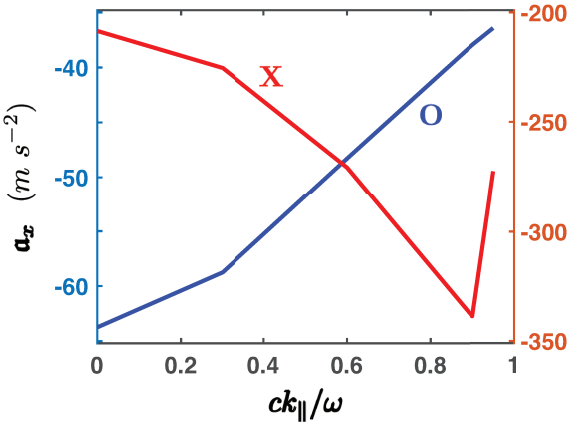

Figure 7. The acceleration of a filament induced by the radiation force of the O mode (left scale) and the X mode (right scale) as function of the index of refraction along the direction of the magnetic field. The density inside the filament is greater than the background density. The negative acceleration means that the filament is being pulled in towards the RF source. For $ck_{\|}/\omega = 0.95$ the X mode is evanescent inside the filament.

4.3.2 *Density inside the filament less than the background density*

In a reversal of the scenario in section 4.3.1, we choose $n_{eb} = 6.5 \times 10^{18}$ m^{-3} and $n_{ef} = 5.0 \times 10^{18}$ m^{-3}; the incident wave is interacting with a filament having a lower density than the background plasma. Figure 8 plots a_x versus $ck_{\|}/\omega$ for incident O (blue) and X (red) modes. The positive acceleration means that the radiation force pushes the lower density filament away from source of the incident wave, further exemplifying the difference in results from planar scattering. The force due to the X mode is larger than due to the O mode; the magnitudes of the two forces having opposite gradients with respect to $ck_{\|}/\omega$.

5 Conclusions

For normal incidence, the radiation force on a planar interface separating two different scalar dielectrics always pushes the interface towards the medium having the higher refractive index. This was first noted by Poynting and his argument was based on the back reaction of the reflected and transmitted waves on the interface. The direction of

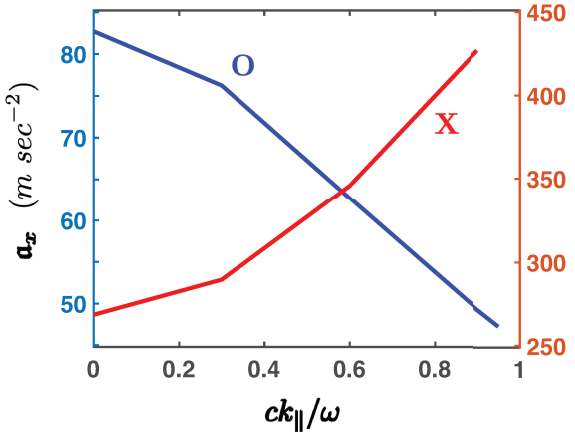

Figure 8. The acceleration of a filament induced by the radiation force of the O mode (left scale) and the X mode (right scale) as function of $ck_{\|}/\omega$. The density inside the filament is less than the background density. The positive acceleration means that the filament is being pushed away from the RF source.

the radiation force had to be opposite to the direction of propagation of the wave with the shorter wavelength – from Planck's relation, the shorter wavelength wave had higher energy and momentum. An analysis based on Snell's law and Fresnel equations leads to the same conclusion.

In a cold magnetized plasma, whose permittivity is a tensor rather than a scalar, the situation is slightly different. First, there are two independent waves that can propagate in a plasma. The number of boundary conditions at the interface are doubled compared to scalar dielectrics. The scattering of any incoming wave at a planar interface will, in general, lead to two reflected and two transmitted waves. Second, unlike scalar dielectrics, over density ranges of interest, the refractive index of electron cyclotron waves decreases with plasma density. However, the physics of the radiation force on a planar interface separating two different plasma densities remains the same as for scalar dielectrics. For normal incidence, the direction of the force due to either the O mode or the X mode is such as to push the interface towards the higher density regions. Since the planar scattering model is applicable anywhere in a fusion plasma, this result leads to an interesting conclusion: the radiation force of the EC waves will lead to peaked density profiles. For the same power flux, the force due to X modes is greater than due to O modes.

A distinct advantage of the planar interface model is that the essential physics can be ascertained using plane waves. The edge region of tokamak plasmas is dominated by blobs and filaments. Any model based on planar scattering lacks validity as geometrical effects such as diffraction, side-scattering, and shadowing come into play. A full wave analysis in which a filament is modeled as a cylindrical plasma forms the basis for studying scattering of EC waves. The radiation pressure on the filament is evaluated using the Maxwell stress tensor. The force of EC waves on the surface of the filament is along the radial direction; there are no shear forces. The radial force is not uniformly

distributed azimuthally, and can deform a filament . However, the integrated force is always such as to pull the filament towards the source of the incoming EC waves or push it away. The former occurs if the density inside the filament is greater than the background density; vice-versa for the latter case. This effect is in direct contrast to that for planar scattering. However, for scattering by planar interfaces or cylindrical filaments, the force due to the X mode is always stronger than that due to the O mode. For filaments, the variation in the force with the parallel index of refraction has opposite gradients for the O and X modes. It is quite possible to experimentally observe the influence of EC waves on filamentary structures, since the induced force leads to large accelerations even for modest input RF powers. The acceleration induced by the EC waves is instantaneous; however, the resulting dynamics of a filament through the background plasma merits a separate study.

The Kirchhoff theory is extensively used in studying the scattering of electromagnetic waves from rough surfaces [17, 18]. In this theory, also referred to as tangent plane or physical optics theory, the electromagnetic field at any point on the surface of a scatterer is assumed to be that on the tangent plane at that point. While not delving into the validity of this approximation, the Kirchhoff theory provides useful insight into the scattering process. In regions where the density fluctuations are not dominated by filaments and blobs, wave scattering by planar interfaces follows Kirchhoff theory. It is a constructive approach to understanding the effect of electron cyclotron waves on density fluctuations. The formalism leads to the conclusion that the radiation force of electron cyclotron waves on core fluctuations will lead to a peaking of the density profile. In experiments on ASDEX-U, peaking of the impurity density profile by EC waves has been observed [19].

For scattering off filamentary structures, the curvature effects are consequential, and the Kirchhoff theory is not applicable. The theoretical modeling has to resort to a full wave description. Electron cyclotron waves affect filaments differently compared to planar interfaces. However, the radiation force still leads to a redistribution of the density in the turbulent plasma.

6 Acknowledgement

AKR was supported by the US Department of Energy Grant numbers DE-FG02-91ER-54109 and DE-SC0018090.

References

[1] A. K. Ram, K. Hizanidis, and Y. Kominis, Physics of Plasmas **20**, 056110-1–056110-10 (2013).

[2] A. K. Ram and K. Hizanidis, Physics of Plasmas **23**, 022504-1–022504-17 (2016).

[3] A. Kohn, E. Holzhauer, J. Leddy, M. B. Thomas, and R. G. L. Vann, Plasma Physics and Controlled Fusion **58**, 105008-1–105008-9 (2016).

[4] Z. C. Ioannidis, A. K. Ram, K. Hizanidis, and I. G. Tigelis, Physics of Plasmas **24**, 102115-1–102115-13 (2017).

[5] A. Snicker, E. Poli, O. Maj, L. Guidi, A. Kohn, H. Weber, G. Conway, M. Henderson, and G. Saibene, Nuclear Fusion **58**, 016002-1–016002-13 (2018).

[6] A. D. Papadopoulos, E. N. Glytsis, A. K. Ram, S. I. Valvis, P. Papagiannis, K. Hizanidis, and A. Zisis, Journal of Plasma Physics **85**, 905850309-1–905850309-20 (2019).

[7] S. I. Valvis, A. K. Ram, K. Hizanidis, P. Papagiannis, A. Papadopoulos, A. Zisis, I. G. Tigelis, and E. Glytsis, Journal of Plasma Physics **84**, 745840604-1–745840604-28 (2018).

[8] S. I. Valvis, A. K. Ram, and K. Hizanidis, Journal of Plasma Physics **87**, 905870612-1-905870612-37 (2021).

[9] D. J. Griffiths, *Introduction to Electrodynamics* (Pearson, Boston, 2013) Chapter 9.3.

[10] J. H. Poynting, The London, Edinburgh, and Dublin Philosophical Magazine and Journal of Science **9**, 393-406 (1905).

[11] A. Bers, *Plasma Physics and Fusion Plasma Electrodynamics, Volume 1* (Oxford, New York, 2016) Chapter 12.

[12] A. Bers, *Plasma Physics and Fusion Plasma Electrodynamics, Volume 1* (Oxford, New York, 2016) Chapter 19.

[13] A. Burnett, Mathematical Proceedings of the Cambridge Philosophical Society **23**, 907-911 (1927).

[14] O. Grulke, J. L. Terry, B. LaBombard, and S. J. Zweben, Physics of Plasmas **13**, 012306-1-012306-7 (2006).

[15] W. K. H. Panofsky and M. Phillips, *Classical Electricity and Magnetism* (Dover, New York, 2005) Chapter 10.

[16] J. A. Stratton, *Electromagnetic Theory* (McGraw-Hill, New York, 1941) Chapter II.

[17] P. Beckmann and A. Spizzichino, *The Scattering of Electromagnetic Waves from Rough Surfaces* (Artech, Massachusetts, 1987) Chapter 3.

[18] J. A. Ogilvy, *Theory of Wave Scattering from Random Rough Surfaces* (CRC Press, Philadelphia, 1991), Chapter 4.

[19] R. M. McDermott *et al.*, Nuclear Fusion **62**, 026006 (2022).